JOURNAL OF CATALYSIS 141, 250–265 (1993)

Intermetallic Pt–Cr Clusters in Zeolites as Models of Bimetallic Aromatisation and Reforming Catalysts

I. Characterisation of Oxidation States, Dispersion, and Local Structure

RICHARD W. JOYNER,*,[1] EFIM S. SHPIRO,†,[1] PETER JOHNSTON,* AND GULIA J. TULEUOVA†

Leverhulme Centre for Innovative Catalysis, Department of Chemistry, University of Liverpool, P.O. Box 147, Liverpool L69 3BX, United Kingdom; and †N. D. Zelinsky Institute of Organic Chemistry, Russian Academy of Sciences, 47 Leninskii Prospect, Moscow 117334, Russia

Received December 12, 1991; revised September 2, 1992

A variety of both structural (EXAFS, XANES, XRD, TEM) and surface-sensitive (XPS, LEISS) techniques have been applied to study the formation, dispersion, composition, and local structure of zeolite-hosted platinum–chromium metal alloys. Both XPS and XANES indicated a two-step reduction of Cr(VI) to Cr(III) and Cr(0) states, while the analysis of EXAFS data demonstrates the formation of platinum–chromium alloy particles after reduction at 823 K. Chromium stabilises small (8–10 Å) platinum particles at lower temperatures (623 K) and when alloyed the particle size increased to 12–20 Å. The Cr/Pt ratio in the alloy is low (<20% chromium), and is independent of the overall Cr/Pt ratio in the ZSM-5, possibly due to space limitations inside the zeolite voids. TEM suggests the formation of some flattened, raft-like metal particles at the external surface of the zeolite. Based on LEISS measurements of surface segregation in a $Pt_{70}Cr_{30}$ alloy film and thermodynamic considerations, a model of the catalyst particles is proposed in which the outermost monolayer consists entirely of platinum and the second shell is enriched in the additive metal, chromium.

1. INTRODUCTION

The study of alloying effects in catalysis is of particular interest due to the importance of bimetallic catalysts in oil refining and other commercial processes (*1–3*). The ensemble model is most frequently used to explain the changes in activity and selectivity of alloys, and it works well for alloys where the active component is diluted by an inactive metal (e.g., Ni–Cu, Pt–Au) (*1*). The case when two active and strongly interacting components are alloyed is more complicated because significant electronic interactions can be expected. The other important factor which is not considered in the ensemble or the ligand model is the coexistence of additives in reduced and nonzerovalent states in many promoted Pt and other noble metal catalysts of commercial interest (*4*). New approaches are under development to understand alloying effects, including the active metal monolayer segregation model (*5*), and the embedded surface molecule approach (*6*). Most input to these models has come from surface science studies (*7–9*) and more careful examination of highly dispersed supported materials is needed.

Our previous data with Pt/ZSM-5 (*10*) and Pt–Cr/ZSM-5 (*11*) convinced us that with zeolites we can prepare a very narrow size distribution of highly dispersed metal particles in a uniform chemical environment, and we also found alloying in bimetallic samples. This has encouraged us to make a more detailed study of Pt–Cr/ZSM-5 catalysts by a variety of physical methods including EXAFS, XANES, XPS, and TEM. The main purpose of this work was to study the

[1] To whom correspondence should be addressed.

0021-9517/93 $5.00

formation of Pt–Cr alloy particles, their structure, composition, and dispersion, and the dependence of performance on the ratio of the two metals in the zeolite. It is also hoped to elucidate the relationship between the characteristics of the bimetallic particles formed and their catalytic activity in hydrogenolysis and aromatisation reactions. Here we report the data on characterisation of Pt–Cr/H-ZSM-5 catalysts. As a model of the possible distribution of platinum and chromium in a bimetallic particle, the surface composition of an unsupported Pt-Cr alloy of similar composition has been investigated by low energy ion scattering spectroscopy (LEISS).

Catalytic data and a discussion of chromium additive effects will be given in Part II (*12*).

2. EXPERIMENTAL

2.1. Materials

The methods of zeolite and catalyst preparation have been described previously (*13*). Samples of NH_4/ZSM-5 (SiO_2/Al_2O_3 ratios 35/1 and 40/1), were exchanged with and subsequently impregnated from aqueous solutions of platinum (II) tetra-ammine dichloride (Pt/ZSM-5 sample). Most of the Pt–Cr catalysts were prepared by simultaneous impregnation from a mixture of solutions of chloroplatinic acid and chromium (VI) oxide, at 273 K. After 24 h the excess solution was evaporated at 353 K and the catalysts were dried in air at 393 K. The metal contents and some other characteristics of the catalysts studied are listed in Table 1.

Calcination was performed in flowing, dry air with a two-stage temperature ramp; the temperature was raised to 620 K at a rate of 1.3 K min^{-1}, held at this temperature for 30 min, raised to the upper temperature (790 K) and held there for 3 h. Before EXAFS, XPS, or TEM studies, the samples were reduced in hydrogen at two temperatures: 623 K for 1–2 h and then at 823–873 K for 1–2 h.

The Pt–Cr alloy was prepared by simultaneous evaporation of the metals onto a Si(111) wafer, to produce a film more than 1 μm thick. The sample was annealed in hydrogen and then in argon at 873 K for 6 h and in vacuum at 623 K, followed by sputtering by argon ions for a short time.

2.2. Procedure

2.2.1. EXAFS. Absorption spectroscopy measurements (EXAFS and XANES) were performed at the SERC Daresbury synchrotron radiation source. Experimental procedures and methods of data analysis have been described before (*10*). Angular momentum dependent phase shifts (l from 0 to 14) were obtained from the Daresbury Laboratory EXAFS data base. For platinum these were refined by comparison to the spectrum of a platinum foil using the programme EXCURV88 and including four shells of neighbours; this multishell analysis approach also optimises the platinum backscattering factor. Phase shifts for chromium and oxygen were used without correction. All analysis was carried out on primary experimental data and Fourier-filtered spectra are presented only as a guide to the eye.

2.2.2. XPS. XPS spectra were recorded with a Kratos XSAM800 spectrometer, as described in Ref. (*14*) C 1*s* (B.E. 285.0 eV) and Si 2*p* (B.E. 103.8 eV) reference lines were used to correct for sample charging. The details of the quantitative analysis are again given in Ref. (*14*). To resolve the Cr 2*p* peaks and the Pt 4*f* + Al 2*p* regions, peak synthesis procedures were applied. The spin–orbit doublet separations were constrained to values known from pure platinum and chromium compounds. In analysing the Cr 2*p* states, the presence of shake-up satellites for Cr(III) was taken into account (*15*).

All supported specimens were treated in an appropriate atmosphere in a specially developed reactor attached to the spectrometer, and they were then transferred to the analysis chamber under vacuum. The vacuum during measurement was better than 5×10^{-9} Torr.

2.2.3. LEISS. $^4He^+$ ions were excited by

TABLE 1

Composition of the Catalysts and Details of Catalyst Preparation[a]

No.	%Pt	%Cr	Initial compound	Preparation procedure	SiO_2/Al_2O_3
1	0.5	0	$Pt(NH_3)_4Cl_2$	Ion exchange + impregn.	35; 40
2	0.5	0.5	H_2PtCl_6 + CrO_3	Coimpregnation	40
3	0.5	0.75	H_2PtCl_6 + CrO_3	Coimpregnation	40
4	0.5	0.75	$Pt(NH_3)_4Cl_2$; CrO_3	Ion exchange (Pt), then impregnation (Cr)	35
5	0.5	1.25	H_2PtCl_6 + CrO_3	Coimpregnation	40
6	0.5	1.75	H_2PtCl_6 + CrO_3	Coimpregnation	40
7	0.5	2.25	H_2PtCl_6 + CrO_3	Coimpregnation	40
8	1.0	0.75	H_2PtCl_6 + CrO_3	Coimpregnation	40
9	0	0.75	CrO_3	Impregnation	35

[a] The zeolite was used in the NH_4 form.

a Minibeam Ion Gun I with energies of 500 or 1000 eV, the pressure of the He flow was 8×10^{-8} Torr, the ion current was less than 100 nA and the irradiated sample area 0.2 cm^2. The scattered ions were analysed with a hemispherical electron analyser operated at reversed polarity. The first LEISS spectrum was recorded after 1–3 min of He^+ bombardment, and repeated scans were taken at 5-min intervals, to look for sputtering effects.

2.2.4. TEM. TEM measurements were made with a JEOL 100CX electron microscope using procedures described in Ref. (*16*). About 300 particles were measured to determine histogram size distributions. The samples were reduced immediately before the TEM measurements.

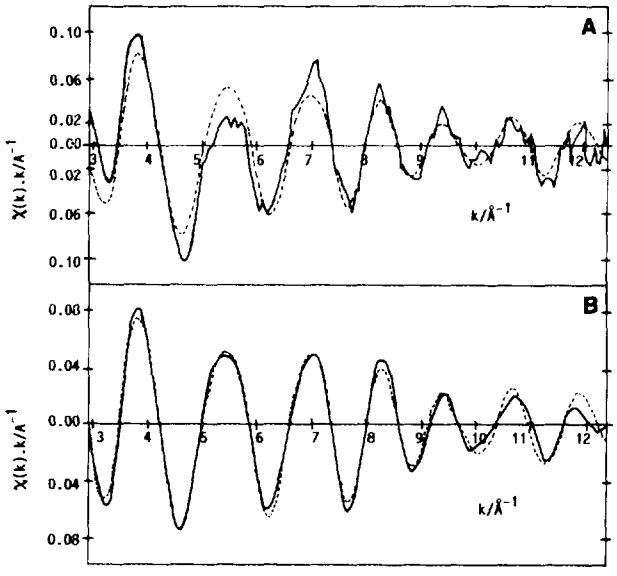

FIG. 1. Platinum L III EXAFS: (A) raw data, and (B) after Fourier filtering, for Pt–Cr/H-ZSM-5 catalyst reduced at 623 K; solid line, experiment; dashed line, calculated using the parameters in Table 2.

TABLE 2

EXAFS Results for a Series of Pt–Cr/ZSM-5 Catalysts Reduced at 623 K

Cat. no	%Cr	Pt–Pt						Pt–O	
		N	R (Å)	N	R (Å)	N	R (Å)	N	R (Å)
2	0.5	7.4 ± 0.5	2.75 ± 0.01	3.4 ± 1	3.91 ± 0.02	2.0 ± 0.7	4.88 ± 0.04	1.3 ± 0.4	1.94 ± 0.03
3	0.75	6.0 ± 0.5	2.74 ± 0.01	3.2 ± 1	3.88 ± 0.02	0.7 ± 0.5	4.76 ± 0.04	0.5 ± 0.2	1.95 ± 0.03
6	1.75	6.5 ± 0.5	2.68 ± 0.01	1.3 ± 1	3.85 ± 0.02	—	—	2.0 ± 0.3	1.90 ± 0.03
8	0.75[a]	9.0 ± 0.5	2.77 ± 0.01	4.1 ± 1	3.92 ± 0.02	7.6 ± 0.7	4.87 ± 0.04[b]	0.9 ± 0.3	1.96 ± 0.03

[a] 1%Pt.
[b] 2a Pt–Pt distance also included in the fit: N = 10; R = 5.48 Å.

3. RESULTS

3.1. EXAFS

Five catalysts containing the same Pt loading (0.5 wt%) but variable amounts of Cr (0.5, 0.75, 1.25, 1.75, and 2.25 wt%) were investigated to determine the influence of the Cr/Pt ratio and reduction temperature, both on particle size and composition. A sixth catalyst contained 1.0% Pt and 0.75% Cr. The results obtained from the EXAFS fitting procedure for the catalysts reduced at 623 K are given in Table 2. Figures 1a and b show the examples of the quality of fit obtained between experimental and calculated EXAFS spectra when three Pt–Pt distances and a single Pt–O distance were included. As in our previous studies of Pt/H-ZSM-5 catalysts (*10*), four shells of neighbours gave the best fit, while exclusion of platinum-oxygen bond led to a significantly worse agreement with experiment, particularly below 8 $Å^{-1}$. The coordination number of the Pt–O bond was different for various samples, but it is important that this did not decrease after additional reduction at the higher temperature 823 K (Table 3). We have checked whether there is any contribution of platinum-chromium bonding in the EXAFS spectra of samples reduced at 623 K. Inclusion of a Pt–Cr distance of ca 2.65 Å did not improve the fit significantly and moreover the Pt–Cr coordination numbers approached zero during the fitting procedure.

The calculated structural parameters for the samples reduced at 823 K are different from those at 623 K: the coordination numbers for all Pt–Pt distances increase and Pt–Cr bonding now contributes to the spectra. This was shown by the improvement of the fit between experimental and calculated EXAFS, as indicated by statistical significance testing (*29*) (Fig. 2). Poor fits were obtained if the Pt–Cr distance was replaced by a Pt–O shell of similar distance. A slight

TABLE 3

EXAFS Results for a Series of Pt–Cr/ZSM-5 Catalysts Reduced at 823 K

Cat. no	%Cr	Pt–Pt						Pt–O		Pt–Cr	
		N	R (Å)	N	R (Å)	N	R(Å)	N	R(Å)	N	R(Å)
2	0.5	7.4 ± 0.5	2.75 ± 0.01	3.4 ± 1	3.91 ± 0.02	2.0 ± 0.7	4.88 ± 0.04	1.3 ± 0.4	1.94 ± 0.03	0.7 ± 0.2	2.66 ± 0.03
3	0.75	7.3 ± 0.5	2.75 ± 0.01	3.7 ± 1	3.88 ± 0.02	2.6 ± 0.7	4.86 ± 0.04	1.9 ± 0.4	1.95 ± 0.03	0.8 ± 0.2	2.67 ± 0.03
4	1.25	7.8 ± 0.5	2.76 ± 0.01	4.7 ± 1	3.91 ± 0.02	4.4 ± 0.7	4.90 ± 0.04	1.1 ± 0.4	1.98 ± 0.03	1.3 ± 0.3	2.69 ± 0.03
5	1.75	7.1 ± 0.5	2.75 ± 0.01	3.6 ± 1	3.86 ± 0.02	2.6 ± 0.7	4.85 ± 0.04	1.5 ± 0.4	1.99 ± 0.03	0.7 ± 0.2	2.66 ± 0.03
6	2.25	7.0 ± 0.5	2.74 ± 0.01	4.5 ± 1	3.88 ± 0.02	3.1 ± 0.7	4.96 ± 0.04	0.5 ± 0.2	1.99 ± 0.03	0.5 ± 0.2	2.55 ± 0.03
7	0.75[a]	9.9 ± 0.5	2.77 ± 0.01	5.2 ± 1	3.91 ± 0.02	9.2 ± 0.7	4.87 ± 0.04	0.8 ± 0.2	1.97 ± 0.03	0.6 ± 0.2	2.71 ± 0.03

[a] 1%Pt.

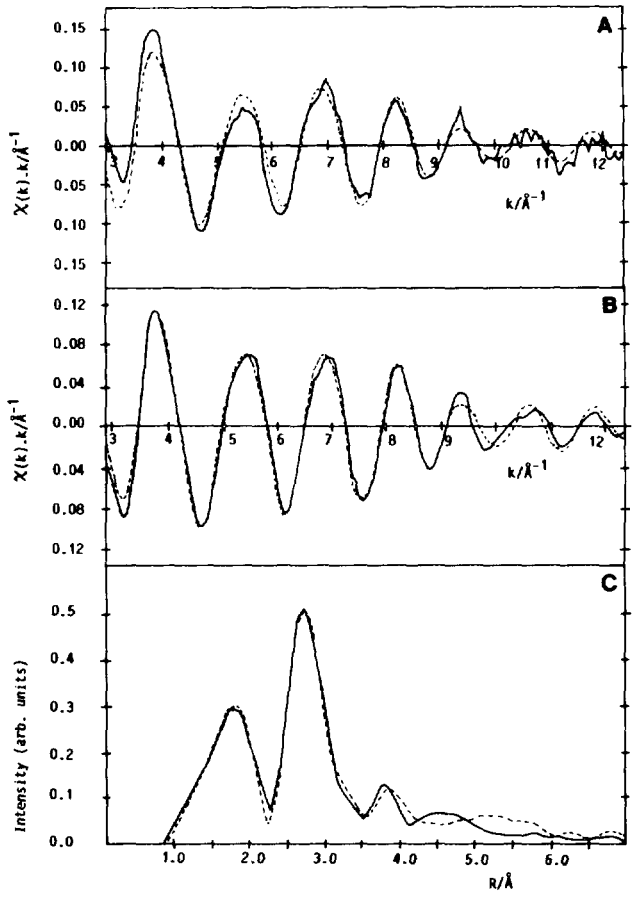

FIG. 2. Platinum L III EXAFS: (A) raw data, (B) after Fourier filtering, and (C) Fourier transform, a Pt–Cr/H-ZSM-5 catalyst reduced at 823 K; solid line, experiment; dashed line, calculated using the parameters in Table 3.

maximum of the coordination number for Pt–Cr was observed as the chromium content increased (Table 3), but the differences in these values for all samples are hardly larger than the error bars. Figure 3 shows the dependence of the Cr/Pt ratio and particle size as a function of chromium loading.

Average particle sizes derived from EXAFS are given in Table 4, and will be referred to in the Discussion.

3.2. *XANES*

Attempts to measure Cr *K*-edge EXAFS were of limited success, because the edge jump was small. Analysis of the spectra obtained for 0.5% Pt–2.25% Cr/ZSM-5 showed a major contribution from Cr–O bonding, which is consistent with the XPS observation that Cr(III) is always the majority species. The Cr XANES region has been examined in more detail to look for valence state changes during reduction (Fig. 4). The most distinct feature in the as received samples is a sharp feature ca. 6 eV below the edge (Fig. 4, curve a). When Pt–Cr samples were reduced at 623 K this peak vanished. Correlation with XPS data and XANES results for reference compounds (*17*) suggest that this pre-edge structure is characteristic of Cr(VI). Additional reduction at 823 K only slightly changed the XANES spectra, the Cr edge position is shifted slightly to

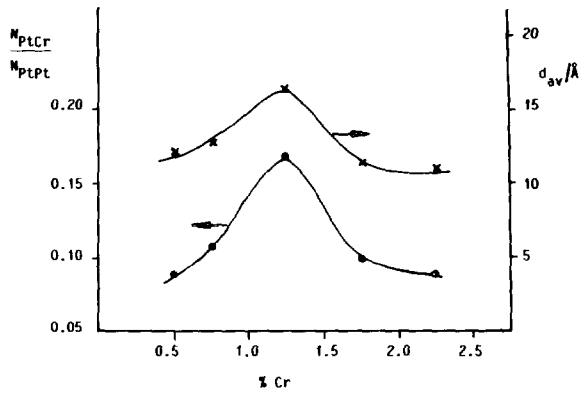

FIG. 3. The dependence of the Cr/Pt ratio in alloy particles (A) and the average size (B), both as a function of chromium loading. The size was estimated for quasi-spherical-shaped particles based on Pt–Pt and Pt–Cr nearest neighbour coordination numbers.

lower energy, but no distinct structure due to metallic chromium was observed. Again, this can be easily understood because the Cr(O) content found by EXAFS and XPS is low with respect to Cr(III).

3.3. XPS

The Pt–Cr samples have been studied at different stages of preparation: after impregnation and drying, after calcination, and following reduction in hydrogen (Table 5). Typical Cr 2*p* spectra are shown for the 0.5 Pt– 0.75 Cr/ZSM-5 sample, which was examined in detail (Fig. 5). Both initial and precalcined samples contain chromium as Cr(VI) (B.E. = 578.5–579.2 eV), and Cr(III) (B.E. = 576.4–577.2 eV). The reduction involves partial decomposition of CrO_3. The

TABLE 4

Average Particle Size of Quasi-spherical-Shaped Particles in Pt–Cr/ZSM-5

Cat. no.	%Cr	N1(Pt–Pt)	Average no. of atoms	Average diameter (Å)	Dispersion (%)
		(a) Reduced at 623 K			
2	0.5	7.4	40 ± 10	10 ± 2	85
3	0.75	6.0	20 ± 5	8 ± 1	90
6	1.75	6.5	22 ± 5	8.5 ± 1	87
8	0.75[a]	9.0	140 ± 30	16 ± 2	60
		(b) Reduced at 823 K			
Cat. no.	%Cr	N1(Pt–Pt) + N1(Pt–Cr)	Average no. of atoms	Average diameter (Å)	Dispersion (%)
2	0.5	8.1	63 ± 10	12.5 ± 2	73
3	0.75	8.1	63 ± 10	12.5 ± 2	73
4	1.25	9.1	150 ± 30	16.5 ± 3	60
5	1.75	8.8	120 ± 25	15 ± 2	67
6	2.25	7.5	40 ± 10	10 ± 2	85
7	0.75[a]	10.5	>600	>22	<50

[a] 1%Pt.

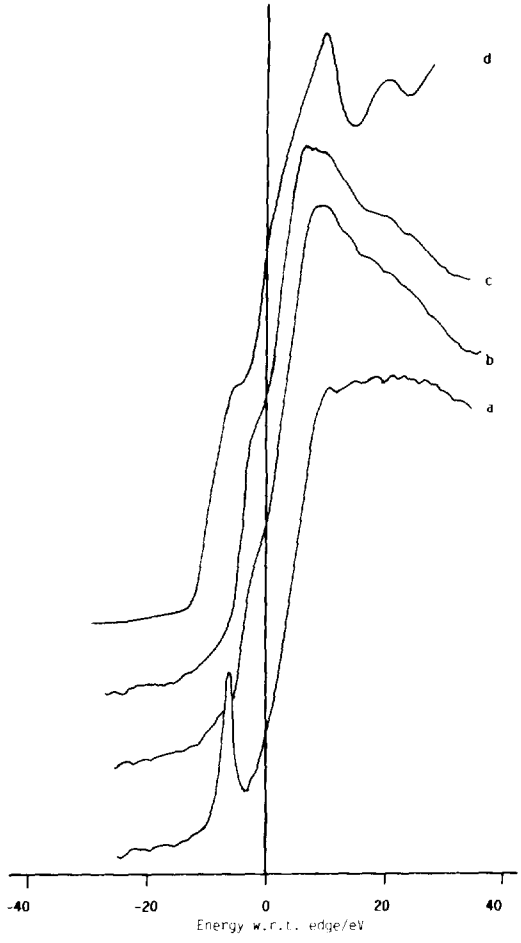

FIG. 4. Cr *K*-edge XANES spectra of 0.5% Pt–0.75% Cr/H-ZSM-5 (a, b, c) and Cr foil (d): (a) calcined in air at 793 K, (b) reduced at 623 K, and (c) reduced at 823 K.

Cr/Si ratio determined by XPS substantially exceeded the average bulk values, which may indicate that initially chromium is predominantly deposited on the external surface of ZSM-5 crystals and only partially enters the channels. With the increase of the Cr bulk content, saturation of the surface Cr/Si ratio was observed (Fig. 6). Based on the data for oxide/pentasil systems, Ga_2O_3/ZSM-5 (*18*), we believe that sintering of chromium oxide and surface segregation both influence the XPS intensity, especially at higher Cr loading. Calcination at 823 K results in a significant decrease of the Cr/Si ratio for all samples, which again is typical for other impregnated metal/ZSM-5 materials (*14*, *18*). This is likely to be the result of a solid state exchange reaction which facilitates additional diffusion of chromium species into the channels. One such species, $(CrO_2)^+$, was detected by ESR in Cr/ZSM-5 and Pt–Cr/ZSM-5 prepared in a similar way (*19*). Cr(VI) and Cr(V) ions in the zeolite seem to be indistinguishable by XPS. From XPS only 25% of the chromium was in the highly oxidised (VI, V) state in the precalcined samples, which may correspond to the fraction located inside the channels.

It is interesting to note that the Cr/Si ratios reached similar values, 0.020–0.026, in all precalcined samples (Table 6). This suggests that a concentration gradient exists between the external surface and the channels of the zeolite and that this promotes the solid state reaction between chromium cations and acidic protons.

Pt(IV) and Pt(II) ions were found in the initial samples in the proportion, 1 : 1. Calcination causes a reduction of Pt(IV) to Pt(II) and of Pt(II) to Pt(O), due to an interaction with ammonia evolved from the NH_4–ZSM-5 zeolite support. This effect is common for many Pt-zeolites (*10*). Because of the partial overlapping of the Pt 4*f* and Al 2*p* lines, measurement of the Pt signal intensity is less accurate than is the case for Cr 2*p*. It is evident (Table 6) that the initial Pt/Si ratios are again higher than the average values, while calcination brings them closer to the bulk figure. Unlike chromium, platinum is rather uniformly distributed over the crystal in the precalcined samples.

XPS data for 0.5% Pt–0.75% Cr/H-ZSM-5 reduced at 623 K show only one chromium state, Cr(III) (Fig. 5). The platinum peaks were decomposed into two components, with $4f_{7/2}$ binding energies of 73.0 and 72.0 eV. These were assigned to Pt (δ^+) and Pt(0) states respectively (*20*). When the reduction temperature was increased to 823–873 K, a new chromium peak with a B.E. of 573.2 eV appeared in the Cr 2*p* spectra, which is

TABLE 5

XPS Analysis of Chromium and Platinum Data

Cat. no	%Pt	%Cr	Treatment	B.E. Cr $2p_{3/2}$ (eV)			B.E. Pt $4f_{7/2}$ (eV)			
				Cr(VI)	Cr(III)	Cr(O)	Pt(IV)	Pt(II)	$Pt^{\delta+}$	Pt(O)
2	0.5	0.75	Initial	578.5(24)[a]	576.4(76)	—	76.2(42)	74.0(58)	—	—
			Air, 793 K	578.4(34)	576.4(66)	—		73.5(40)		71.9(60)
			Air, 793 K + H_2, 823 K	—	577.5(89)	573.6(11)	—	—	73.0(44)	72.1(56)
5	0.5	1.25	Initial	579.0(35)	577.2(65)	—	76.2(57)	74.0(43)	—	—
			Air, 793 K	579.0(25)	577.2(75)	—		74.1(72)		72.6(28)
			Air, 793 K + H_2, 823 K	—	577.5(87)	573.4(13)	—	—	73.0(39)	71.8(61)
6	0.5	1.75	Initial	578.5(30)	577.3(70)	—	75.9(37)	73.9(63)	—	—
			Air, 793 K	578.5(30)	576.7(70)	—		74.1(72)		72.3(28)
			Air, 793 K + H_2, 823 K	—	577.2	573.2	—	—	73.0(60)	72.0(40)
7	0.5	2.25	Initial	579.2(43)	577.0(57)	—	76.0(62)	74.2(38)	—	—
			Air, 793 K	578.9(25)	576.5(75)	—		74.0(65)		72.5(35)
			Air, 793 K + H_2, 823 K	—	577.1	573.3	—	—	73.1(50)	71.9(40)

[a] Figures in parentheses show the percentage of certain oxidation states.

associated with Cr(0) (*15*). The fraction of metallic chromium in the Pt–Cr samples depends on the preparation procedure and varies from 10 to 30% (*13*). In the case of samples 3 and 4, the degree of reduction did not exceed 10–12%. Approximately the same amount of Cr(0) was found in 0.5% Pt–1.25% Cr/ZSM-5 sample. In samples with higher chromium content, determination of reduction degree was difficult because of the large contribution of the Cr(III) intensity to the total Cr 2*p* signal. All reduced samples have Pt 4*f* binding energies which are more positive (+1.0–1.3 eV), than for metallic platinum. This is characteristic of small metallic particles on supports and is due to relaxation effects and possibly to some charge transfer between the metal and the support (*14*, *20*).

3.4. *Transmission Electron Microscopy*

TEM micrographs and the particle size distribution histogram obtained for samples containing 0.75 and 1.25% Cr suggest that the detectable particles are in the range of 8–24 Å diameter, with a most probable value of 16 Å (Fig. 7A and B). No larger particles were observed. The particles can be divided into two fractions, particles embedded into the zeolite structure (5–15 Å in diameter) and larger (10–20 Å) "flattened" particles, which give a weak contrast and are preferentially located on the external surface or in channel mouths. That particles larger than 24 Å in size were not observed is unusual for metal/zeolite system with particles at the external surface. This indicates a rather strong interaction of the flattened phase with the support, which prevents its sintering.

3.5. *LEISS of Pt–Cr Alloy*

Because of the appreciable content of non-reduced chromium and its preferential location on the external surface, neither the Cr/Pt ratio in the alloy nor its concentration profile in the catalysts can be measured by surface analysis techniques. The EXAFS results suggest that the alloy particles are rich in Pt, and that the Cr/Pt ratio does not exceed 0.33, a value which is characteristic of the Pt–Cr intermetallic Pt_3Cr. Most of the samples contain even less chromium, with Cr/Pt in proportions from 2/10 to 1/10. Thus, we can consider them as diluted chromium solutions in platinum. Based on what is known of surface segregation in bulk di-

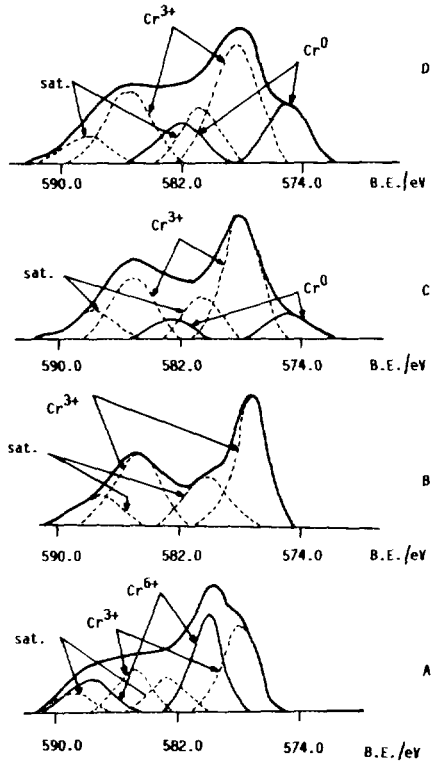

FIG. 5. XPS Cr 2p spectra of 0.5% Pt–0.75% Cr/H-ZSM-5 catalysts: (A) calcined, (B) reduced at 623 K, (C) reduced at 823 K, and (D) sample prepared from $Pt(NH_3)_4Cl_2$ and CrO_3 and reduced at 823 K. Dashed curves show the presence of certain components, obtained by peak synthesis procedures.

luted alloys (*21*), we can expect surface enrichment with platinum. For strongly interacting components such as Pt–Ni, Pt–Ti, or even Pt–Co, a two-layer sandwich structure has been proposed with the top layer mainly consisting of platinum and the second layer enriched in the additive (*7, 8, 21*). Such a structure is very likely for Pt–Cr, because the mixing energy of Pt–Cr lies between that of Pt–Ti and Pt–Ni, and is larger than that for Pt–Co.

To seek support for this model we have studied the surface composition of a Pt–Cr alloy film by LEISS (Fig. 8). X-ray diffraction indicated that the sample was a solid solution of chromium in platinum with the unit cell parameter, $a = 0.3861 \pm 0.0005$ nm. The surface of the silicon wafer substrate was the (111) plane, and it was found that the Pt–Cr film was mainly oriented in the {111} direction. The bulk composition is close to 70% Pt/30% Cr, and the unit cell parameter is in excellent agreement with alloys of similar composition (*24*). No ordered intermetallic phase was observed. XPS measured at normal photoemission angle gave a very similar composition. After the sample was reduced in hydrogen and cleaned by argon bombardment, XPS showed the presence of peaks due to platinum and chromium with binding energies close to those of the corresponding metals.

The Pt/Cr ratios obtained by LEISS in the most surface-sensitive regime (500 eV ion energy) exceed 12 (Fig. 8). It then slightly decreased to 10, after 30-min He^+ scattering. Quantitative determinations of the Pt/Cr atomic ratio were made, based on reference data (*24*). We calculate that the Pt/Cr sensitivity factors ratio will not exceed two in our conditions. This gives a *minimum* Pt/Cr ratio of 6–7, i.e., the top layer is significantly enriched in platinum. Following the procedure proposed in Ref. (*8*), we have also measured the Pt/Cr intensity ratio at 1 keV, allowing us to probe two

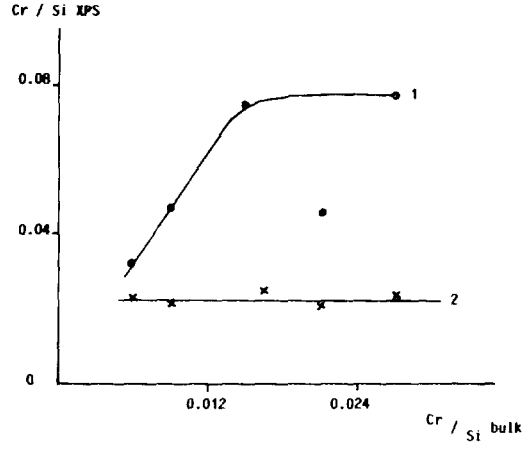

FIG. 6. The relation between surface and bulk Cr/Si ratio in Pt–Cr/H-ZSM-5 catalysts: (1) initial samples and (2) calcined or reduced samples.

TABLE 6

XPS Analysis of Surface Composition

Cat. no.	%Cr	Treatment	Pt/Si × 10^3	Cr/Si × 10^3	Pt/Cr	Pt(s)[a]/Pt(b)[b]	Cr(s)[a]/Cr(b)[b]
2	0.5	Initial	—	32	—	—	5.3
		Air, 793 K	—	22	—	—	3.6
3	0.75	Initial	2.93	47	0.06	1.88	3.36
		Air, 793 K	2.66	21	0.13	1.71	1.50
		H_2, 823 K	1.24	20	0.06	0.79	1.43
5	1.25	Initial	3.60	75	0.05	2.31	5.0
		Air, 793 K	1.61	25	0.06	1.03	1.67
		H_2, 823 K	2.50	22	0.12	1.60	1.47
6	1.75	Initial	1.95	46	0.04	1.24	2.19
		Air, 793 K	2.42	20	0.12	1.54	0.95
		H_2, 823 K	1.90	26	0.07	1.21	1.23
7	2.25	Initial	2.67	77	0.04	1.69	2.85
		Air, 793 K	1.51	23	0.07	0.96	0.85
		H_2, 823 K	1.02	26	0.04	0.65	0.96

[a] Surface.
[b] Bulk.

layers. The value obtained, 4–5, indicates that the second layer is likely to be enriched in chromium, with respect to the bulk. Thus the LEISS measurements confirm platinum surface enrichment for the Pt–Cr solid solution. It is quite probable that when an ordered Pt–Cr intermetallic structure is formed, the enrichment will be even stronger so that the first layer will consist only of platinum.

4. DISCUSSION

We will consider the influence of chromium on the dispersion of the metallic particles in the zeolite matrix, discuss the Pt–Cr alloy particles that result from high-temperature reduction, and examine the structure and composition of these particles and of the unsupported alloy that we are considering as a model system.

When the catalysts are heated in hydrogen at 623 K, chromium is reduced only to the 3+ oxidation state, and the metallic particles formed contain only platinum. For 0.5% platinum loading, the nearest neighbour coordination numbers show the formation of particles of rather similar size for all samples studied, 8–11 Å (Table 4a). The sample with the higher platinum content (1%) had twice as large particles, in good agreement with previous results (*10*). Comparison with results for Pt/H-ZSM-5 catalysts treated in a similar way (*10*, *25*), shows that the presence of chromium ions stabilises the platinum dispersion on reduction at 623 K. Instead of particles with a mean diameter of 15 Å, particles of 8–10 Å size are noted for the Pt/Cr catalysts. This may reflect anchoring of platinum particles at Cr^{3+} ions located in the channels, and possibly prevention of platinum migration to the external surface by partial pore blocking due to the presence of chromium oxide.

The relatively large amount of Pt–O bonding has been discussed before (*10*), and we believe that it reflects the location of the particles close to the zeolite framework. A recent transmission electron microscopy study has demonstrated that platinum particles up to 2 nm in diameter can be accommodated in voids in the ZSM-5 structure (*26*). It seems likely that the ZSM-5 lattice fragments in a similar way to that proposed for faujasite (*26*), since release of aluminum

from the framework is frequently observed for ZSM-5 in this temperature range (*30, 31*). We can be clear that the observed Pt–O coordination does not result from the presence of platinum oxide since the Pt–O coordination number, rather than decreasing, shows a slight increase on heating the catalyst in hydrogen at 823 K, where platinum oxides are readily reducible.

The most striking feature of the results when the catalysts are reduced at the higher temperature (823 K) is the appearance of platinum–chromium bonding. We again note that the EXAFS theory/experiment comparison for catalysts reduced at the lower temperature is not markedly improved by the introduction of Pt–Cr bonding, while, for materials reduced at the higher temperature, the improvement in the fit is statistically very significant. The interatomic distance observed is in the range expected for a Pt–Cr alloy, i.e. between that for metallic Pt–Pt and Cr–Cr bonding. The small changes reported in the chromium XANES spectra, which are dominated by the presence of Cr(III), are difficult to interpret, but are not inconsistent with the presence of metallic chromium. Finally, and very importantly, the XPS results observed after reduction at this temperature now indicate the presence of Cr(0). Reduction of Cr(III) is induced by the presence of platinum, since no reduction is observed for Cr_2O_3/H-ZSM-5 catalysts (*32*), and the metallic chromium state is stabilised by alloying with platinum.

Some sintering of the particles is observed as a result of reduction at this higher temperature since the coordination numbers increase. Determination of the average particle size from the EXAFS measurement is not straightforward, however, since the chromium coordination numbers in the alloy cannot be determined. Only a small part of the chromium is reduced to the metallic state so detailed analysis of the chromium *K*-edge EXAFS would not be informative. If the alloy particles are homogeneous the average total coordination number for either platinum or chromium will be given by [CN(Pt–Pt) + CN(Pt–Cr)] and the relative magnitude of CN(Pt–Pt) and CN(Pt–Cr) will be an indication of their concentration ratio in the alloy. [CN(Pt–Cr) indicates the number of chromium atoms coordinated to the average platinum atom in the catalyst; CN(Cr–Pt) would indicate the reverse.] This would suggest that the catalyst particles are relatively dilute in chromium and with average particle diameters indicated in Table 4b, calculated assuming spherical shape. If there is chromium aggregation or segregation within the particles the average size will be greater than that calculated. This effect is not expected to be significant, because of the nature of platinum–chromium bonding. The existence of the ordered intermetallic compound Pt_3Cr demonstrates that Pt–Cr bonding is stronger than Cr–Cr bonding, so chromium aggregation will not be favoured at equilibrium. The situation in small catalyst particles is difficult to predict, although the relatively high temperatures used here should allow efficient mixing, so arguments based on equilibrium considerations may be reasonable. We also note that there is good agreement between the average particle size of the 0.75% chromium catalyst determined by transmission electron microscopy (Fig. 7), and that calculated from the analysis of EXAFS coordination numbers assuming no chromium aggregation or segregation (Table 4b). Both TEM and EXAFS therefore suggest that the average particle size is now very similar to that reported earlier for chromium free, 0.5% Pt/H-ZSM-5 catalysts. Particles with an average size exceeding 22 Å were observed for the 1% Pt–0.75% Cr/H-ZSM-5 catalyst.

In comparison with catalysts prepared without chromium (*10*), all of the materials studied here show very low values of the $\sqrt{3}a$ coordination number (where a is the nearest neighbour distance). This is unexpected, especially as the values for the $\sqrt{2}a$ shell of neighbours remain high. A possible explanation is the presence of some raft-like particles, with a structure based on the (100)

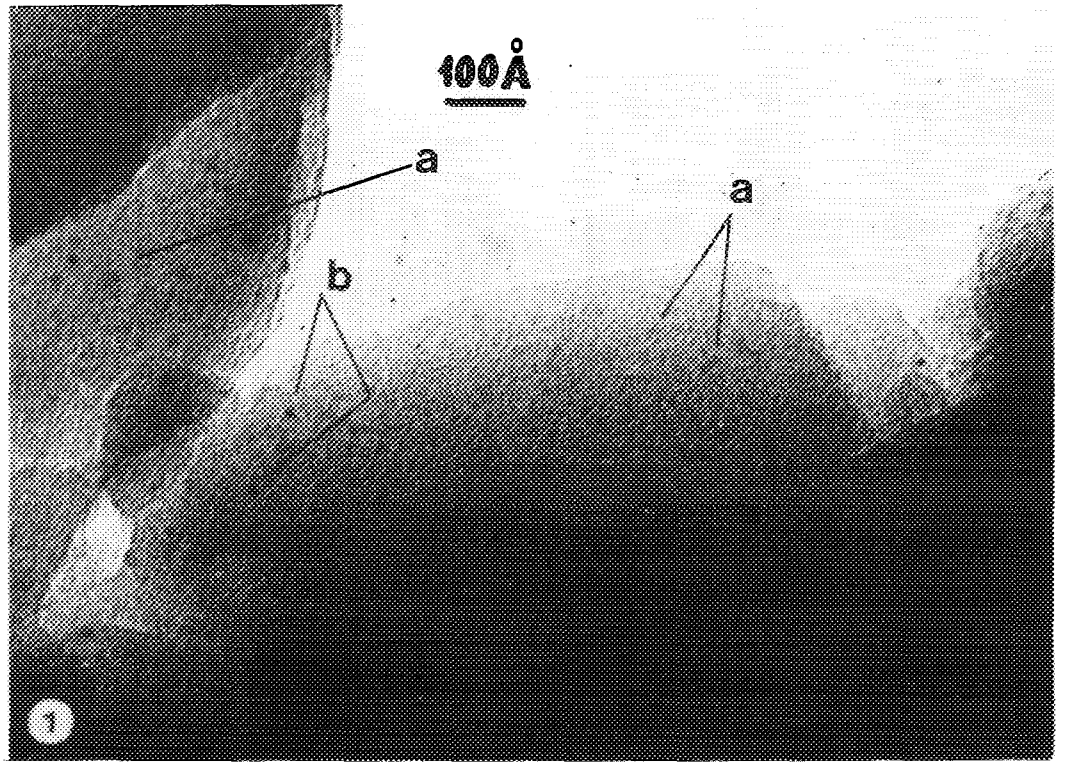

FIG. 7A. TEM micrographs of Pt–Cr/H-ZSM-5 catalysts reduced at 823 K: (1) 0.5% Pt–0.75% Cr and (2) 0.5% Pt–1.25% Cr. The arrows show particles of different size and location ((a) clusters within 5–10 Å inside the zeolite interior and (b) "surface" particles 10–20 Å in size); (3) 0.5% Pt–1.25% Cr. This is representative of flattened particles located at the external surface.

plane of the face-centered cubic crystal structure. A single layer of this structure would contain $\sqrt{2}a$ as the next nearest distance, but the $\sqrt{3}a$ distance would be systematically absent. Alternatively, the low value of the $\sqrt{3}a$ coordination number might reflect beating between the $\sqrt{3}a$ shells, respectively, of Pt–Pt and Pt–Cr, due to differences in backscattering factors.

Electron microscopy provides evidence for the occurrence of both spherical and flattened particles. These appear to be orientated along the (001) direction of the zeolite structure and are mostly observed at the external surface of the catalysts. This shape of particle could contribute to the anomalous non-nearest neighbour coordination numbers observed by EXAFS. The presence of chromium may help to stabilise the dispersion of small particles at the external surface of the zeolite, where sintering leading to large particles is commonly observed.

There is a discrepancy between the amount of metallic chromium determined by XPS and that deduced from the EXAFS coordination numbers, with XPS suggesting a significantly greater amount of Cr(0) than would be deduced from the EXAFS coordination numbers. The XPS method is surface sensitive, and can usefully be applied only to those samples with low chromium loadings, where the small contribution from Cr(0) can be resolved from the dominant Cr(III) signal. By contrast, EXAFS provides a true average of the environment of all platinum atoms in the sample studied, but will not

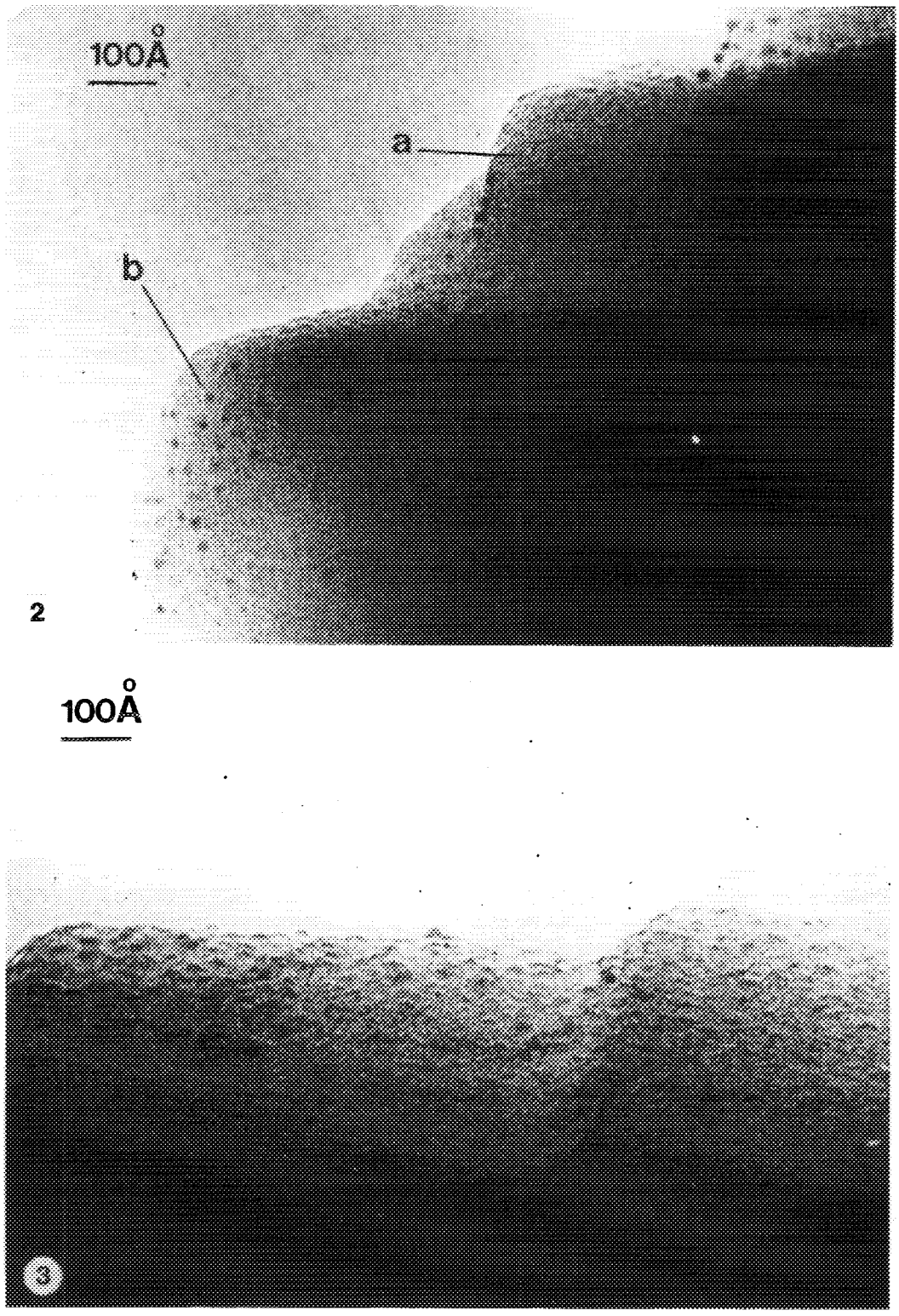

FIG. 7A—*Continued*

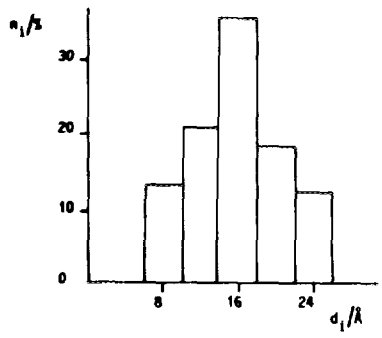

FIG. 7B. TEM size distribution histogram for the 0.5% Pt–0.65% Cr/H-ZSM-5 catalyst, reduced at 823 K.

detect any chromium not associated with platinum. Analysis of data from both methods involves mathematical curve-fitting procedures that have reasonably high associated errors, so that the exact extent of the discrepancy is difficult to evaluate. It seems likely that the chromium content of particles near the external surface may be higher than that in the bulk of the zeolite lattice. We do not consider that there is a separate metallic chromium phase present, since reduction to Cr(0) is not observed in Cr_2O_3/ZSM-5 catalysts (*32*), although reduction by hydrogen spillover from platinum particles cannot be ruled out. However, our catalytic results are not consistent with the presence of isolated metallic chromium particles, which would be expected to be highly active in alkane hydrogenolysis (see Ref. (*5*) and Part II (*12*)). In the following we assume that EXAFS analysis provides the more accurate indicator of alloy particle composition, since it refers only to chromium associated with platinum, and provides a true average over the whole sample.

It is interesting and surprising that the composition of the small Pt–Cr alloy particles appears only slightly affected by varying the amount of chromium in the catalyst. There is an increase in the Pt–Cr coordination number as the chromium content is raised from 0.5 to 1.25% but it appears to fall as the chromium loading is further increased. All of the Pt–Cr coordination numbers are very similar, within the relatively large experimental errors. It appears that there is a limit to the solubility of chromium in the platinum particles, which is signifi-

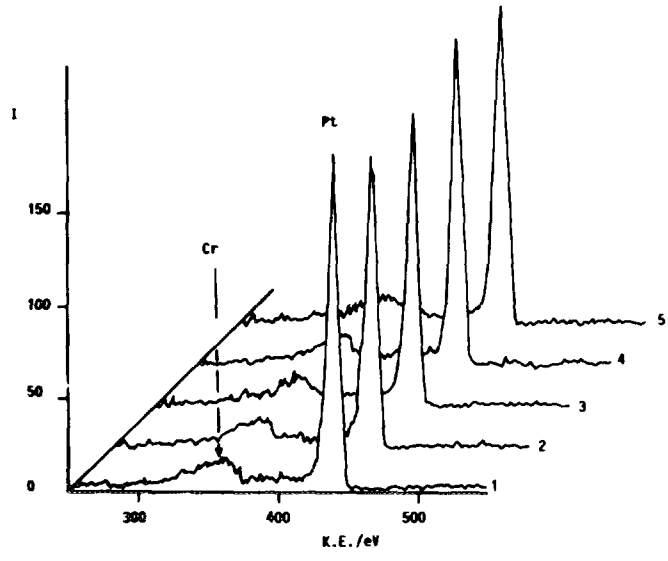

FIG. 8. Time-dependent LEISS spectra of Pt 70% Cr 30% alloy: (1) 2 min, (2) 7 min, (3) 12 min, (4) 18 min, and (5) 25 min of He^+ exposure.

cantly less than that for bulk Pt–Cr alloys, 71% (*27*).

Several factors may be responsible for the apparent limit on chromium solubility. The results show that small particles containing only platinum are formed first, on reduction at 623 K. At the higher temperature, therefore, chromium must both be reduced and migrate into the alloy particles. XPS results suggest that chromium oxide diffusion into the zeolite channels may be limited, and that this controls the availability of chromium for reduction and alloying. The results of Borona *et al.* (*28*), who studied the formation of Pd–Cr alloy particles, suggest that the chemistry of catalyst preparation is unimportant in determining alloy composition, and this is unsurprising in view of the high reduction and calcination temperatures employed. The constraints that the zeolite lattice places on particle growth may also be important, even considering the voids that are generated by particle formation. There is some evidence that, when there are larger particles, they contain more chromium, for example in the sample containing 1.25% Cr. Electron microscopy suggests that the larger particles are located at the external surface of the zeolite.

Our preliminary EXAFS study suggested that the alloy particles were smaller than reported here, with an average diameter of less than 10 Å (*11*) and containing typically 13 atoms. For most of the samples studied here the average number of atoms is close to 55, that of the next stable cubooctahedron configuration. The cause of this difference in particle size is not clear, but it may reflect differences in the Si/Al ratio of the zeolites used or small differences in preparation procedure.

We have previously proposed a novel model for the structure of particles in bimetallic and alloy platinum catalysts for gasoline reforming, in which the surface monolayer is composed entirely of platinum, with the additive composition enriched in the immediate subsurface layer (*5*). Structural support for this model was provided from a number of surface science studies of Pt–Ni, Pt–Co, and Pt–Ti alloys (*7, 8, 21, 22*), and it was also argued that the model unified the wide range of additives that can be used and rationalised our catalytic observations. It is recognised that such a detailed model cannot be directly probed by the catalyst characterisation techniques used here, although none of the results reported is inconsistent with the proposal. To examine the applicability of the model specifically to Pt–Cr alloys a low energy ion scattering spectroscopy study has been carried out for a Pt 70%, Cr 30% alloy film, orientated in the (111) direction. This shows marked enrichment of the surface, with a minimum platinum content of ca 85%. On this basis, it seems probable that the surface of a Pt–Cr intermetallic compound would consist entirely of platinum. Also of relevance are the results obtained when 1-keV ions, which are thought to probe approximately two surface layers (*8, 24*), are used in the LEISS experiment. The composition obtained is now closer to the bulk value, suggesting that the second layer of the alloy is enriched in chromium.

We believe that the results obtained on the bulk alloy (111) are relevant to the likely structure of small alloy particles, while recognising that surface composition in both the bulk and in small particles is crystal plane dependent. The reduction tempera-

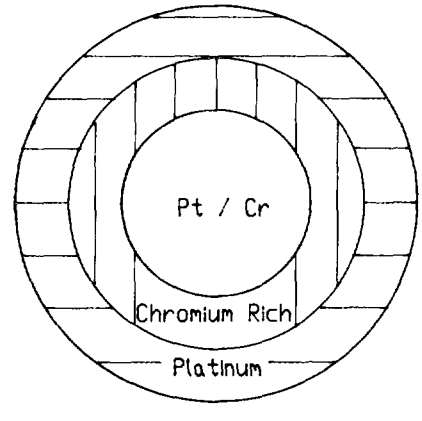

FIG. 9. Model of the bimetallic Pt–Cr particle in the H-ZSM-5 supported catalyst.

tures used, 823 K, is quite sufficient to permit effective mixing of the components in the particle and to establish an equilibrium composition. We therefore reiterate the structural model that we have proposed before (Fig. 9), where the exterior surface of the particles is composed entirely of platinum but the next layer is enriched in chromium compared to the bulk composition. For the small clusters of interest here, the central core will contain only a small number of atoms, irrespective of whether the particles are spheres or rafts, although the model is clearly not applicable to a raft only a single atom in thickness. If the particle was a raft containing two layers, the chromium-rich core would comprise the interior atoms in the layer in contact with the support.

ACKNOWLEDGMENT

We thank Dr. V. J. Zaikovskii for the TEM measurements and Mrs. N. S. Telegina for assistance in obtaining LEISS spectra and XRD measurements on the Pt–Cr alloy. We are grateful to Mr. R. Bilsborrow for assistance with the X-ray absorption studies. We thank SERC and the Royal Society for financial support. Helpful comments were received from a referee.

REFERENCES

1. Ponec, V., *Adv. Catal.* **32,** 149 (1983).
2. Clarke, J. K. A., and Rooney, J. J., *Adv. Catal.* **25,** 125 (1976).
3. Sinfelt, J. H., "Bimetallic Catalysts." Wiley, New York, 1982.
4. Sachtler, W. M. H., *J. Mol. Catal.* **25,** 1 (1984).
5. Joyner, R. W., and Shpiro, E. S., *Catal. Lett.* **9,** 233 (1991).
6. Joyner, R. W., Catal. Today, **12,** 355 (1992); *in* "Proceedings, 10th International Congress on Catalysis Budapest, 1992." Akademiai Kiadó, Budapest, p. 1.
7. Bardi, U., Atrei, A., Ross, P. N., Zanazzi, E., and Rovida, G., *Surf. Sci.* **211–212,** 441 (1989).
8. Paul, J., Cameron, S. D., Dwyer, D. J., and Hoffmann, F. M., *Surf. Sci.* **177,** 121 (1986).
9. Bowker, M., and Joyner, R. W., submitted for publication.
10. Shpiro, E. S., Joyner, R. W., Minachev, Kh. M., and Pudney, P. D. A., *J. Catal.* **127,** 366 (1991).
11. Joyner, R. W., Minachev, Kh. M., Pudney, P. D. A., Shpiro, E. S., and Tuleuova, G. J., *Catal. Lett.* **5,** 257 (1990).
12. Shpiro, E. S., Joyner, R. W., Johnston, P., and Tuleuova, G. J., *J. Catal.*, **141,** 266, (1993).
13. Shpiro, E. S., Tuleuova, G. J., Zaikovskii, V. I., Tkachenko, O. P., Vasina, T. V., Bragin, O. V., and Minachev, Kh. M., *Stud. Surf. Sci. Catal.* **46,** 143 (1988).
14. Minachev, Kh. M., and Shpiro, E. S., "Catalyst Surface: Methods of Studying." CRC Press, Boston, 1990.
15. Grunert, W., Shpiro, E. S., Feldhaus, R., Anders, K., Antoshin, G. V., and Minachev, Kh. M., *J. Catal.* **100,** 138 (1986).
16. Ryndin, Yu. A., Chernyshev, V. I., Zaikovskii, V. I., Yurchenko, E. N., and Ermakov, Yu. I., *React. Kinet. Catal. Lett.* **21,** 125 (1982).
17. Bianconi, A., Garcia, J., Benfatto, M., Marcelli, A., Natoli, C. R., and Ruiz-Lopez, M. F., *Phys. Rev. B* **43,** 6885 (1991); Gibbs, T. C., *J. Mater. Chem.* **2,** 57 (1992).
18. Tkachenko, O. P., Shpiro, E. S., Vasina, T. V., Preobrazhensky, A. V., Bragin, O. V., and Minachev, Kh. M., *Bull. USSR Acad. Sci.* **314,** 668 (1990).
19. Kucherov, A. V., and Slinkin, A. A., *Zeolites* **7,** 38 (1987).
20. Bragin, O. V., Shpiro, E. S., and Preobrazhensky, A. V., *Appl. Catal.* **27,** 1219 (1986).
21. Mukherjee, S., and Moran-Lopez, J. J., *Surf. Sci.* **189,** 1135 (1987).
22. Gauthier, Y., Joly, Y., Baudoing, R., and Rundgren, J., *Phys. Rev. B* **35,** 6216 (1987).
23. Engels, S., Lausch, H., Peplinski, B., Wilde, M., Morke, W., and Kraak, P., *Appl. Catal.* **55,** 93 (1989).
24. Stuurmeijer, E. P. Th. M., and Boers, A. L., *Surf. Sci.* **43,** 309 (1973).
25. Kampers, F. W. H., Engelen, C. W. R., van Hooff, J. H. C., and Koningsberger, D. C., *J. Phys. Chem.* **94,** 8574 (1990).
26. Schulz-Ekloff, G., *Stud. Surf. Sci. Catal.* **69,** 65 (1991).
27. Hansen, M., "Constitution of Binary Alloys," 2nd ed. McGraw–Hill, New York, 1958.
28. Borona, A., Moraweck, B., Massardier, J., and Renouprez, A. J., *J. Catal.* **128,** 99 (1991).
29. Joyner, R. W., Martin, K. J., and Meehan, P., *J. Phys. C (Solid State Phys.)* **20,** 4005 (1987).
30. Topsøe, N.-Y., Joensen, F., and Derouane, E. G., *J. Catal.* **110,** 404 (1988).
31. Lago, R. M., Haag, W. O., Mikovsky, R. J., Olsen, D. H., Hellring, S. D., Schmidt, K. D., and Kerr, G. T. *in* "Proceedings, 7th International Zeolite Conference, Tokyo, 1986," p. 677.
32. Wichterlova, B., Krajcihova, L., Tvaruzkova, Z., and Beran, S., *J. Chem. Soc. Faraday Trans 1* **80,** 2639 (1984).